Theor Chem Acc (2002) 108:71–84
DOI 10.1007/s00214-002-0365-7

Theoretical
Chemistry Accounts

*Feature article*

# Computational modeling of enzymatic keto-enol isomerization reactions

**Isabella Feierberg, Johan Åqvist**

Department of Cell and Molecular Biology, Uppsala University, Biomedical Center, Box 596, 751 24 Uppsala, Sweden

Received: 3 January 2002 / Accepted: 13 May 2002 / Published online: 29 July 2002


**Abstract.** Catalysis of proton abstraction from nonacidic carbon atoms adjacent to a carbonyl or carboxylate group is a fundamental reaction in enzymology that has been extensively studied during the last few decades. Enzymes catalyzing these reactions, which normally involve labile enolic intermediates, need to overcome large p$K_a$ differences between the reacting groups as well as high intrinsic free-energy barriers. Here, we present an overview of results from recent computer simulation studies of keto-enol isomerization reactions catalyzed by the enzymes glyoxalase I, triosephopsphate isomerase and ketosteroid isomerase. For all three enzymes it is found that electrostatic stabilization of the transient enolate intermediates, either by charge–charge interactions or by hydrogen bonding, accounts for the main part of the activation free-energy barrier reduction. Another catalytic effect observed in all cases is the reduction of the reorganization energy by the enzyme active site. Some other factors that have been proposed to be important for these reactions are also discussed and evaluated.

**Key words:** Enzyme catalysis – Keto-enol isomerization – Empirical valence bond method – Molecular dynamics – Free-energy calculations

## 1 Introduction

The origin of the catalytic efficiency of enzymes that catalyze proton abstraction from nonacidic carbon atoms adjacent to a carbonyl/carboxylate group has been the subject of considerable experimental and theoretical research in recent years [1–12]. Such enzymes include, for example, triosephosphate isomerase (TIM), enolases, citrate synthase, mandelate racemase, glyoxalase I (GlxI), rubisco and ketosteroid isomerase (KSI). The corresponding uncatalyzed reactions in aqueous solution are usually extremely slow, which can be understood from the high-energy nature of the conjugate anionic intermediates or transient species resulting from proton abstraction as well as high intrinsic free-energy barriers. Acetone can be considered as an illustration of the general energetic problem faced by the catalysts where a p$K_a$ of about 20 has been measured for deprotonation of this compound in solution [13]. While the substrates of the enzymes mentioned previously in some cases have somewhat lower p$K_a$s than acetone, the nonacidic nature of the carbon atom from which proton abstraction occurs is a general feature of these enzymic reactions. In view of the fact that a number of structurally and evolutionary unrelated enzymes have arrived at different catalytic machineries for dealing with these reactions, it is of fundamental interest to understand the general catalytic principles that this particular type of chemistry requires.

An early attempt to rationalize the rapid enzyme-catalyzed proton abstraction rates in the keto-enol type of isomerization reactions was made by Gerlt and Gassman [2]. They argued that the proton abstraction by an active-site general base catalyst (apparently required in all enzymes of this category) should be concerted with protonation of the carbonyl/carboxylate group by a general acid residue and that this type of mechanism would offer a major catalytic advantage. This proposal was criticized by Guthrie and Kluger [3], who pointed out that the problem is primarily a thermodynamic one, pertaining to the enol as well as the enolate, and that the former species need not, in general, be much stabler than the conjugate anion. These authors instead favored electrostatic stabilization of the enolate as a mechanism for increasing the acidity of the substrates, but hydrogen bonding alone was not considered sufficient [3].

In a subsequent article, Gerlt and Gassman instead invoked the concept of unusually strong hydrogen bonds (with stabilization energies of 20 kcal mol$^{-1}$ or greater, as sometimes found in the gas phase) to the substrate oxygen as the main source of catalysis [4]. In analogy with strong gas-phase hydrogen bonds involving anionic acceptors, these so-called low-barrier hydrogen bonds

*Correspondence to*: J. Åqvist
e-mail: aquist@xray.bmc.uu.se

(LBHBs) were assumed to be characterized by essentially a single-well potential for the proton or a double-well potential with a barrier low enough for it to have a significant covalent interaction with both the donor and acceptor [4, 5]. A corollary of this hypothesis is that the proton at room temperature would be localized to neither of the heavy atoms, but rather would be shared equally between them, and that the donor–acceptor distance would be very short. The existence of LBHBs in enzymes has since been widely debated and the discussion has revolved around interpretation of NMR spectra and crystal structures as well as numerous theoretical calculations [14–19]. The differing opinions and results can perhaps best be characterized in terms of whether an enzyme active-site environment is viewed as being gas-phase-like or not. If it is, there is no conceptual problem with the spread out charge distribution of an LBHB and a strong (unscreened) interaction, while in a polar environment it is always the case that localized charges are more stabilized than delocalized ones and dielectric screening also attenuates the strength of the hydrogen bond. In this respect, it is probably significant that gas-phase quantum mechanical calculations (sometimes also including a low-dielectric continuum) on small model systems often find LBHBs [19], while they never seem to be observed in quantum mechanics/molecular mechanics calculations on enzymes in a solvent environment [9, 10, 14]. It is, however, a fact that mutation experiments have never produced an effect due to removal of a hydrogen bond of the magnitude originally proposed.

Regarding the enzymes that catalyze the keto-enol type of isomerizations it is also of interest to note that, in fact, all of them seem to achieve stabilization of the transient or intermediate enolate-like species through strong interactions either with hydrogen bond donors or with active site cationic groups (metal ions, lysine or arginine side chains). While the differences in the substrate p$K_a$ values could perhaps explain some of the differences in the choices of catalytic groups, it is still noteworthy that some of these enzymes can achieve efficient transition-state stabilization by hydrogen bonds alone when others are crucially dependent on divalent metal ions to accomplish the same task.

Here, we discuss recent empirical valence bond (EVB) simulations of three different enzyme reactions of the type just described, namely those catalyzed by GlxI, KSI and TIM. We will further try to illustrate how the simulation methodology used can provide quantitative insight into the contributions of different potentially important effects for the catalytic rate enhancement.

## 2 Computational methods

Our treatment of the enzymic proton-transfer reactions is based on the EVB formulation where an elementary proton-transfer process can be described in terms of two (impure) VB states,

$$\begin{aligned} \psi_1 &= D - \mathrm{H}A \ , \\ \psi_2 &= D^- \mathrm{H} - A^+ \ , \end{aligned} \tag{1}$$

that also represent a possible mixing with a higher-energy resonance form of the $D^-\,H^+\,A^-$ type [20, 21]. The effective EVB Hamiltonian involves the diagonal (diabatic) energies of the two resonance structures and off-diagonal terms that describe the resonance interactions between the states. The generalization to multistep (or concerted) reactions, of course, requires more resonance structures to be included, but is otherwise straightforward. Each diagonal energy function is given by

$$\begin{aligned} H_{ii} = \varepsilon_i = V^{(i)}_{\mathrm{bond}} + V^{(i)}_{\mathrm{angle}} + V^{(i)}_{\mathrm{torsion}} \\ + V^{(i)}_{\mathrm{nb,rr}} + V^{(i)}_{\mathrm{nb,rs}} + V_{\mathrm{ss}} + \alpha^{(i)} \ , \end{aligned} \tag{2}$$

where the first three terms describe the intramolecular potential energies of the reacting fragments (donor and acceptor molecules/residues plus possibly extra groups of the enzyme, cofactors, etc.) by Morse bond potentials, harmonic three-atom angle bending and proper and improper torsional angle functions. The fourth term denotes nonbonded van der Waals and electrostatic interactions within and between the reacting fragments. The fifth and the sixth terms describe the interactions between the reactants and the surrounding environment and the potential energy of the surrounding enzyme/water system, respectively, in terms of a standard force field. The last term of the Hamiltonian represents the intrinsic gas-phase energy of the given resonance structure with all fragments at infinite separation, i.e. noninteracting.

Combination of the EVB representation of the reaction potential surface with the molecular dynamics (MD) free-energy perturbation (FEP) technique allows us to drive the system between VB states $i$ and $j$ and sample system configurations along the way [20, 21]. At each configuration, the ground-state energy is obtained as the lowest eigenvalue of the secular equation. Besides the diagonal (diabatic) energies, the ground state also depends on the off-diagonal matrix elements, $H_{ij}$, representing the nonadiabatic mixing of the VB states. These are typically described by an exponential function of the type [20–23]

$$\begin{aligned} H_{ij}(r_{XY}) = A_{ij} \exp\Big[-\mu_{ij}\Big(r_{XY} - r^{\ddagger}_{XY}\Big) \\ -\eta_{ij}\Big(r_{XY} - r^{\ddagger}_{XY}\Big)^2\Big] \end{aligned} \tag{3}$$

or a simplified version thereof, where $r_{XY}$ denotes the distance between the donor and acceptor. These off-diagonal terms as well as the gas-phase energy shifts, $\alpha^{(i)}$, are often determined by fitting the EVB potential surface to available data regarding the uncatalyzed reaction in solution [20, 21, 23]. With such a procedure the solution free-energy surface is thus calibrated to reproduce experimental data and the parameters $\alpha^{(i)}$ and $H_{ij}$, although they in principle pertain to the gas-phase surface, are not explicitly parameterized for the gas-phase reaction. The advantage with this approach is that possible errors in the solvation free energies (that relate the gas-phase reaction to the energetics in solution) of the reaction fragments can be taken care of by the calibration. This is useful since an accurate gas-phase parameterization could easily be "destroyed" by errors in the reactant and product solvation energies of a few kilocalories per mole, thereby rendering the resulting solution surface much less accurate. However, it is, of course, recommendable to examine the energetics of the thermodynamic cycle obtained through this type of calibration procedure to ensure that it is consistent. This was done, for example, in Ref. [24] for the carbonic anhydrase reaction, where the accuracy of the gas-phase reaction free energy was found to be within 1 kcal mol$^{-1}$ of the experimental value. The consistency of the EVB calibration is further discussed in the simulations of TIM below.

The calculations of free-energy profiles follow the FEP procedure described in Ref. [23]. For an elementary proton-transfer step, the two VB states are "connected" via a set of intermediate mapping potentials $\varepsilon_m = \lambda^m_i \varepsilon_i + \lambda^m_j \varepsilon_j$, where $\varepsilon_i$ is given by Eq. (2) and $\lambda^m_i + \lambda^m_j = 1$. The mapping vector $\vec{\lambda}_m = (\lambda^m_i, \lambda^m_j)$, defining a linear combination between the two potentials, changes between the values (1, 0) of reactants and (0, 1) of products. The reason for representing $\vec{\lambda}_m$ as a vector is that, in general, more than two states may be involved in defining the FEP path [25]. The free energy associated with changing $\varepsilon_i$ to $\varepsilon_j$ in $n$ discrete steps is obtained as

$$\Delta G\left(\vec{\lambda}_n\right) = \Delta G\left(\vec{\lambda}_0 \rightarrow \vec{\lambda}_n\right) = -\beta^{-1}\sum_{m=0}^{n-1} \ln\langle \exp[-\beta(\varepsilon_{m+1} - \varepsilon_m)]\rangle_m \ , \quad (4)$$

where $\beta = 1/kT$ and the average $\langle\rangle_m$ is evaluated on the mapping potential surface $\varepsilon_m$. The free-energy profile $\Delta G(X)$ corresponding to trajectories moving on the actual ground-state potential, $E_g(X)$, is calculated from the umbrella sampling expression:

$$\Delta G(X) = \Delta G\left(\vec{\lambda}_m\right) - \beta^{-1}\ln\left\langle \delta(X - X')\exp\left\{-\beta\left[E_g(X) - \varepsilon_m(X)\right]\right\}\right\rangle_m \ , \quad (5)$$

where the reaction coordinate, $X = \Delta\varepsilon = \varepsilon_i - \varepsilon_j$, is the energy gap between the two diabatic surfaces [20, 21, 23].

In some of the calculations discussed below the effects of quantum mechanical nuclear motion are explicitly evaluated through the centroid path integral technique [26, 27]. Each quantized particle is then represented by a closed ring (or necklace) of quasiparticles (beads), which are sequentially connected by harmonic springs and each experiences a fraction of the external potential acting on the real particle. The effective quantum mechanical potential of such a quantized particle is given by

$$V_q = \frac{mP}{2}\frac{(kT)^2}{h^2}\sum_{j=1}^{P}\left(\mathbf{x}_{j+1} - \mathbf{x}_j\right)^2 + \frac{1}{P}\sum_{j=1}^{P} V_{cl}\left(\mathbf{x}_j\right) \ , \quad (6)$$

where $P$ is the number of quasiparticles (with coordinates $\mathbf{x}_j$) in the necklace, $m$ is the mass of the real atom and $V_{cl}$ is the classical potential on the quasiparticle. For the interaction between quantized atoms, quasiparticle $j$ in one necklace interacts only with the corresponding $j$th bead in the other. Here, we utilize the fact that the motion of the center of mass (or centroid, denoted by $\bar{\mathbf{x}}$) of each quantized particle can be rigorously separated from the fluctuations of the beads around the centroid [27]. We then use a Monte Carlo (MC) procedure to generate configurations of the latter motions together with classical MD simulations of the full system including the centroids [28]. The umbrella sampling formula now becomes

$$\Delta G(X) = \Delta G\left(\vec{\lambda}_m\right) - \beta^{-1}\ln\left\langle \delta(X - X')\left\langle \exp\left\{-\frac{\beta}{P}\sum_j\left[E_g\left(\mathbf{x}_j\right) - \varepsilon_m(\bar{\mathbf{x}})\right]\right\}\right\rangle_{fp}\right\rangle_m \ , \quad (7)$$

where the sum runs over all quasiparticles in each necklace and the average $\langle\rangle_{fp}$ is taken over the free particle necklace distributions. In the calculations reported for GlxI below, the path-integral treatment was employed with limited sets of quantized particles that included atoms up to 1–3 neighbors (forming bond angles) with the transferred proton, in any of the two VB states.

MC configurations were generated for each isotope (using 20 and 64 beads for each quantized atom), starting from a configuration with all beads on top of each other, and first equilibrated for 4M steps. The maximum step sizes for the beads (in the $x$, $y$ and $z$ directions) ranged from 0.02 Å for $^{16}O$ to 0.1 Å for $^{1}H$, yielding an acceptance ratio of 40–50%. For each classical MD step ($\Delta t = 1$ fs) five new MC configurations were then used for energy-averaging (trajectories with one and ten MC steps per MD step were also calculated [28]). With 5,000 MD steps for each FEP point and energy sampling every five steps, this yields a total of 5,000 necklace configurations used per FEP point. This procedure was found to give good convergence 28]. It can thus be noted here that a relatively small number of necklace configurations appears sufficient for sampling the free particle distributions, which is reasonable since the number of beads is not very large and their mutual interaction is simple.

One of the main advantages of the EVB method is that the gas-phase free-energy difference, $\Delta\alpha_{ij} = \alpha^{(j)} - \alpha^{(i)}$, between two VB states, $\Psi_i$ and $\Psi_j$, and the off-diagonal element, $H_{ij}$, describing the resonance interaction between these states, can be determined by calibrating the calculated free-energy profile of an appropriate reference reaction in solution against experimentally derived reaction free energies and activation barriers. In this way, the reaction energetics of the enzyme-catalyzed reaction can be compared directly to its nonenzymatic counterpart in aqueous solution. The EVB calibration procedure for the different enzyme reactions is described elsewhere [8, 11]. MD calculations were carried out using the Gromos87 force field as implemented in the program Q [29] and supplemented with AM1 (Mulliken) charges for "nonstandard" chemical moieties. Further details regarding simulation procedures are given in Refs. [8, 11, 23, 28].

## 3 Simulations of different enzymes

In discussing simulations of enzyme-catalyzed keto-enol isomerization reactions we will start by considering GlxI, which is an example of a divalent metal dependent enzyme, where the metal cation plays a major role in catalysis. We will then turn to TIM, which does not contain any metal, but has one positively charged lysine residue interacting with the substrate. Finally, we will discuss simulations of KSI, in which case no positive charges are present in the active site. Besides trying to elicit the basic features of the catalytic effect in these enzymes, we will also examine a few of the many general propositions for the source of enzyme catalytic power that have been put forward.

### *3.1 Glyoxalase I*

GlxI catalyzes the formation of *S*-D-lactoylglutahione from the nonenzymatically formed hemithioacetal of methylglyoxal and reduced glutathione (Fig. 1). This is the first of two enzymatic reactions in which toxic methylglyoxal is converted to D-lactic acid [30]. Besides a divalent metal cation, the enzyme thus requires a glutathione molecule as a cofactor which spontaneously reacts to form the actual hemithioacetal substrate. The crystal structure of the human enzyme in complex with a relevant (glutathione derivative) analogue of the expect-

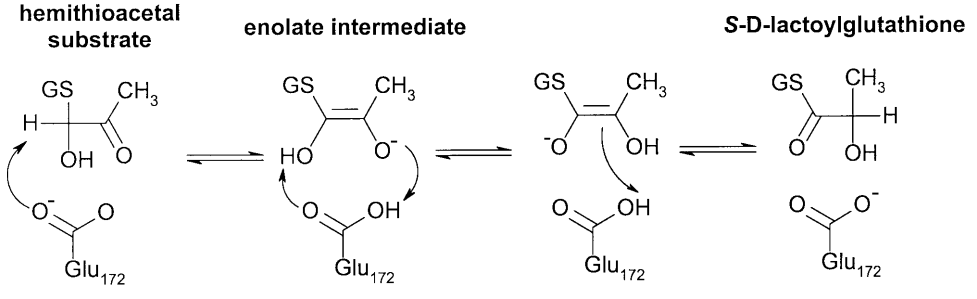


**Fig. 1.** Mechanism of the reaction catalyzed by glyoxalase I (*GlxI*). *GS* denotes the glutathione part of the hemithioacetal substrate

ed *cis*-enediol/enediolate intermediate has recently been determined [31] and provides the starting point for our simulations. Here, we only consider the first and rate-limiting [30] reaction step, in which the C1 proton is abstracted by the general base residue Glu172. In the crystallographic structure both of the hemiacetal oxygen atoms as well as Glu172 together with another glutamate, a histidine and a glutamine residue are coordinated to the active-site metal (Fig. 2).

The energetics of the uncatalyzed reaction in water corresponding to the first catalytic step in GlxI can be quite accurately estimated from p$K_a$ values and the experimental free-energy relationship between activation barriers and the donor–acceptor p$K_a$ difference in Ref. [8]. The values obtained are $\Delta G^{\ddagger}_{wat} = 22.1$ kcal mol$^{-1}$ for the activation barrier and $\Delta G^{0}_{wat} = 12.8$ kcal mol$^{-1}$ for the reaction free energy [11]. The EVB potential (Eqs. 2, 3) is thus fitted to these data by simulations of the solution reaction followed by iterative calculations of the free-energy profile as described in Refs. [20, 21]. It should be pointed out here that the resulting reaction surface implicitly includes the quantum mechanical zero-point energy (ZPE) and tunneling effects, since it is fitted to experimental data, but that these effects are assumed to be the same in the enzyme reaction as in water. This approximation will be quantitatively examined later with the use of path integral simulations.

After constructing the effective EVB potential by calibration against the uncatalyzed reaction, the proton-transfer process is simulated in the active site of human GlxI (Fig. 2). These simulations were done with a spherical system of radius 18 Å containing both protein and explicit water molecules [29]. The calculated free-energy profiles are shown in Fig. 3 for the reaction in water and in the solvated enzyme, where three different active site metal ions ($Zn^{2+}$, $Mg^{2+}$ and $Ca^{2+}$) were examined. The calculated free-energy barriers yield rate

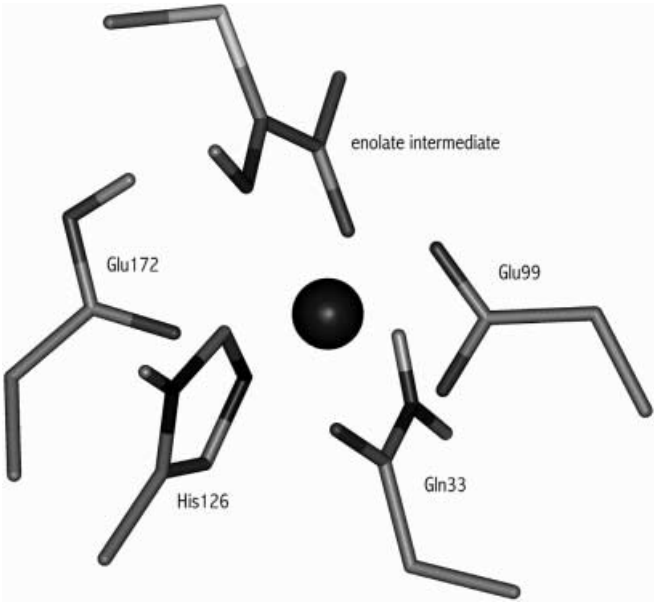


**Fig. 2.** Average molecular dynamics (*MD*) structure of the enolate species in the active site of GlxI with $Mg^{2+}$ as a cofactor

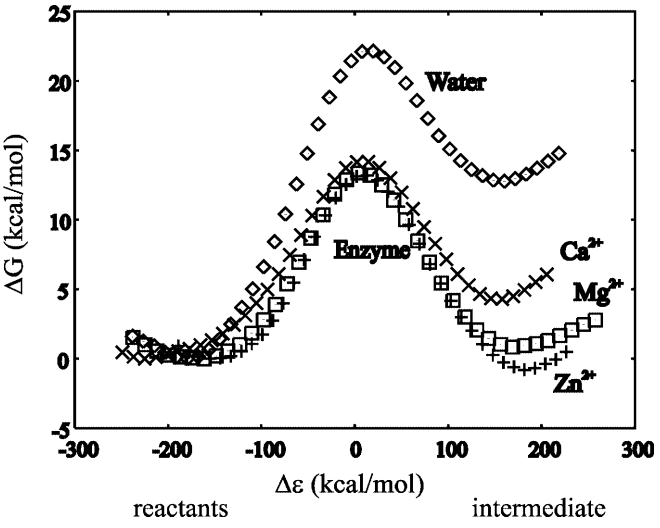


**Fig. 3.** Calculated free-energy profiles for proton abstraction by a glutamate in solution and in GlxI with $Zn^{2+}$, $Mg^{2+}$ and $Ca^{2+}$ bound to the active site

constants of approximately 300–1,500 s$^{-1}$, which is in very good agreement with the observed rate of GlxI and the relative insensitivity of this enzyme to the catalytic metal species is also reproduced [11, 30].

In this case, it is evident that electrostatic stabilization of the high-energy intermediate enolate ion is the main source of catalysis. A detailed analysis of the interactions with the substrate in the active site, compared to the uncatalyzed reaction, shows that the metal is by far the most important stabilizing factor. In the case of $Mg^{2+}$, for example, evaluation of its effect on the apparent p$K_a$ difference between Glu172 and the substrate shows that the ion accounts for more than half of the relative stabilization of the enolate. By artificially shifting the reaction free energy of the uncatalyzed reaction in solution to the calculated value in the enzyme, which is done by simply varying $\Delta\alpha_{ij} = \alpha^{(j)} - \alpha^{(i)}$, one can easily examine whether the entire barrier reduction is explained just by modulation of the relative p$K_a$s. This procedure amounts to the addition of a hypothetical negative constant energy term to the enolate in solution, which mimics the differential effect of the enzyme interactions on the substrate and intermediate without changing the form of the diabatic free-energy functions in solution. The shift in $\Delta\alpha_{ij}$ thus required in order to make the solution reaction free energy coincide with that in the enzyme is about 13 kcal mol$^{-1}$, which, as expected, agrees with the overall stabilization of the enolate in the enzyme. The result of such a calculation is shown in Fig. 4, where it can be seen that about 70% of the activation barrier reduction originates from stabilization of the enolate intermediate. The remaining 3 kcal mol$^{-1}$ is not due to a lowering of $\Delta G^0$, but is a pure transition-state stabilization that is found to originate from the reduction of the reorganization energy of the reaction [11]. This phenomenon will be analyzed and discussed further later.

An issue that has received considerable attention in recent years is the role of quantum mechanical effects in enzyme catalysis, particularly hydrogen tunneling [32]. There are several promising routes for addressing such

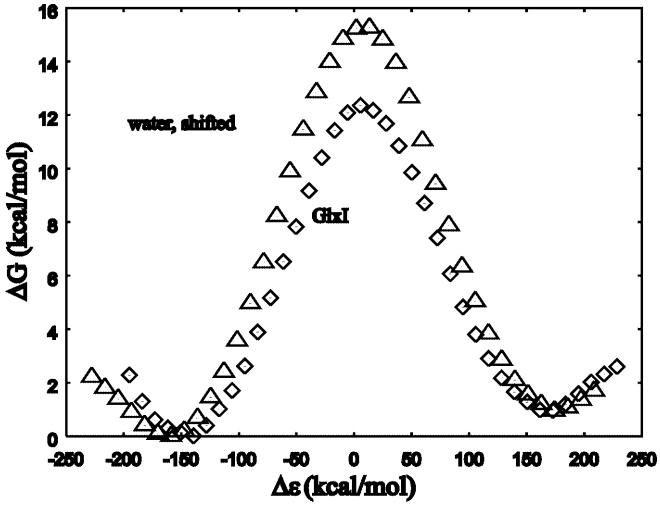


**Fig. 4.** Evaluation of the contribution from enolate stabilization to the overall catalytic effect on the rate-limiting step in GlxI. By "artificially" shifting the relative p$K_a$s of donor and acceptor in the uncatalyzed solution reaction (by varying $\Delta\alpha$), so that the reaction free energy coincides with the result for the enzyme, the remaining difference in the activation barrier that is not explained by stabilization of the intermediate can be quantified

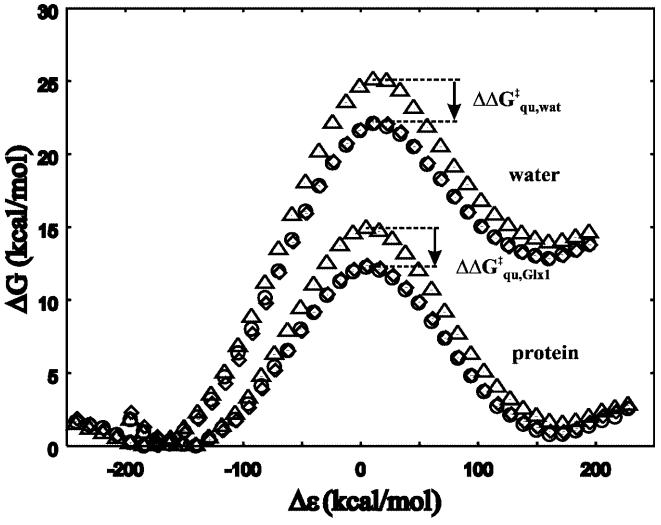


**Fig. 5.** Comparison of free-energy profiles from path integral and classical EVB simulations of the rate-limiting step in GlxI. The path integral results are denoted by *diamonds* (calibration: $\Delta\alpha_{12} = 6.6$, $H_{12} = 40.0$ kcal mol$^{-1}$, with $\Delta\alpha$ uncorrected for intramolecular nonbonded terms), while the classical simulations that implicitly include quantum effects through the calibration are given by *circles* ($\Delta\alpha_{12} = 5.6$, $H_{12} = 44.3$ kcal mol$^{-1}$). The results of the classical simulations are also shown (*triangles*) without accounting for zero-point energy and tunneling effects, by utilizing the path integral calibration ($\Delta\alpha_{12} = 6.6$, $H_{12} = 40.0$ kcal mol$^{-1}$) of the uncatalyzed reaction in water. The stability of the simulations was examined by using either three or six quantized atoms as well as using 20 or 64 beads per atom. The overall quantum effects (on both $\Delta G^{\ddagger}$and $\Delta G^0$) in water and in the enzyme obtained from the different protocols differ by less than 0.2 kcal mol$^{-1}$

problems by computational approaches [12, 27]. The path integral technique outlined earlier provides a very useful strategy for exploring the effects of quantizing the nuclear motion on, in principle, any analytical potential energy surface. As already indicated, it is also of importance to examine the common assumption in EVB simulations that ZPE and tunneling contributions do not change appreciably between solution and enzyme reactions. This is, of course, particularly relevant for proton- and hydride-transfer reactions which are likely to have substantial tunneling contributions to the rates.

The results of comparing classical and path integral EVB simulations of the rate-limiting proton abstraction in GlxI and in solution are shown in Fig. 5. By calibration of the uncatalyzed path integral free-energy profile, which now has explicit ZPE and tunneling contributions, against the experimental data in solution, the magnitude of these effects can be estimated directly by comparison with the classical profile obtained with the same EVB parameterization (the reason why the path integral simulations in solution require a new parameterization is that the quasiparticles are now "moving" on the ZPE surface rather than on the classical one below it. Furthermore, the change in ZPE and also tunneling effects are largest in the barrier region, so the main difference between the classical and path integral parameterizations is in the $H_{ij}$ term). For the solution reaction this yields an overall quantum effect corresponding to a lowering of the effective free-energy barrier of 2.5 kcal mol$^{-1}$. The separation of ZPE and tunneling contributions from this type of calculation is not so straightforward (see later) but it is clear that the main part of the barrier overestimation for the classical case originates from the neglect of the ZPEs [26]. The most important result from Fig. 5 is, however, that the magnitude of the contributions from quantized motion to the activation barrier is almost exactly the same in the enzymic and the aqueous reaction. Thus, while ZPE and tunneling effects significantly influence the rate of proton transfer (by a factor of about 100) the effects are virtually identical in the enzyme and in water and the overall contribution to catalysis is negligible. The same conclusion has been reached for other enzyme systems as well [33, 34].

It is also important to emphasize that the classical EVB profile in the enzyme, obtained using the classical parameterization of the solution reaction (as in Fig. 3), is practically indistinguishable from the path integral free-energy profile obtained with the corresponding path integral calibration of the uncatalyzed reaction. This clearly shows that idea of using an effective (classical) EVB potential that implicitly incorporates quantum effects on the reaction rate, through parameterization against experimental data, works well. One may note that calibration of the EVB surface against ab initio calculations should, therefore, take these effects into account and the same is true for QM/MM approaches [35].

Since the EVB simulations reproduce the observed reaction rate of GlxI very well we were motivated to examine also the primary H/D/T kinetic isotope effects (KIEs) by path integral calculations. Experimental measurements comparing methylglyoxal and perdeuteriomethylglyoxal as well as phenylglyoxal and α-dueteriophenylglyoxal substrates have shown that the primary deuterium isotope effect on the catalytic rate is about 3

in the yeast enzyme [36]. A similar value was obtained with methylglyoxal substrates for the human enzyme, while phenylglyoxal in that case yielded a H/D KIE of 6.6 [37]. These data also strongly suggest that the initial proton abstraction from the hemithioacetal substrate is the rate-limiting step of the reaction. The results of path integral simulations of H/D/T abstraction in the initial reaction step of GlxI are shown in Fig. 6 and the KIEs and summarized in Table 1. The calculated value of the H/D KIE is 5.0 ± 1.3 for the enzyme reaction, which is thus in good agreement with the experimental observations. It is also of interest to note that the simulations of H/D/T abstraction from the hemiacetal in aqueous solution (free-energy profiles not shown) yield a primary H/D isotope effect of 3.6 ± 0.7, which coincides almost perfectly with the observed value of 3.8 for the hydroxide ion catalyzed methyl- versus perdeuteriomethylglyoxal substrate reaction in water [36]. The acetate-catalyzed reaction of acetone in water yields an experimental H/D KIE of 3.76 and a H/T KIE of 8.3 [38] and we also note that these values are close to those obtained from the present calculations.

Finally, in view of the recently proposed importance of hydrogen tunneling in enzyme reactions [32], it is interesting to evaluate the so-called Swain–Schaad exponents [38], which have been used as indicators of tunneling effects. In the semiclassical picture, where the KIEs only originate from the differences in the ZPE (assuming no shift in transition structures between isotopes), the ratio between the primary H/T and D/T KIEs is predicted just from the masses to obey the relation $\ln(H/T)/\ln(D/T) = 3.3$. In particular, if this ratio is significantly larger than 3.3 it would indicate that transfer of the lighter proton has a substantial contribution from tunneling. The values obtained for the Swain–Schaad exponent using the data of Table 1 are 4.8 ± 1.0 in the enzyme and 3.2 ± 0.3 and 3.4 for the solution and gas-phase reactions, respectively. Since the exponent for the water reaction is close to the semiclassical predicted value and the D/T KIEs have similar values in the enzyme and in water, the larger value of the exponent in the enzyme would seem to reflect enhanced $H^+$ tunneling. Comparison of the H/D and H/T KIEs with the solution reaction, however, suggests that the effect in terms of apparent activation free energy is quite small (0.2 kcal $mol^{-1}$ or less) and is barely significant in view of the convergence error bars of the calculations (±0.2 kcal $mol^{-1}$).

Taken together, the results clearly indicate that the overall contribution of quantum mechanical effects to the catalytic rate enhancement in GlxI, using the solution reaction as a reference, are insignificant compared to the electrostatic stabilization of the enolate and the reduction of the reorganization energy. The magnitude of ZPE and tunneling contributions to the absolute rates are, however, not negligible and amount to an effective barrier reduction of about 2.5 kcal $mol^{-1}$ both in the enzyme and in water. The calculations also show that the influence of zero-point vibrations is more important than tunneling in this respect.

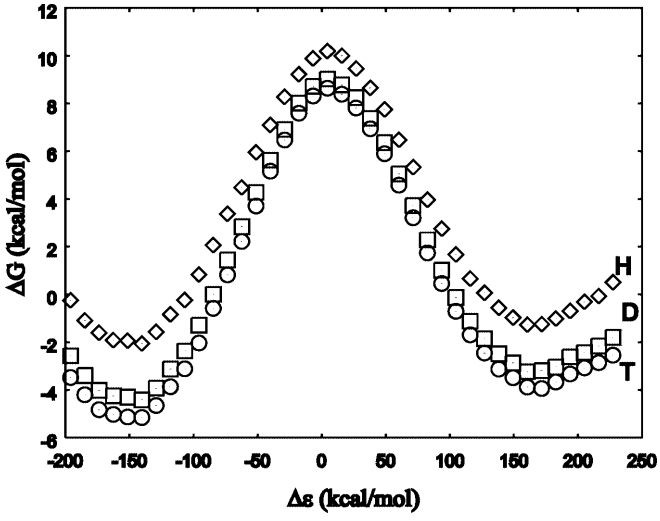


**Fig. 6.** Free-energy profiles from path integral simulations in the enzyme with the H, D and T isotopes denoted by *diamonds*, *squares* and *circles*, respectively

**Table 1** Calculated primary kinetic isotope effects (*KIE*) for the proton-transfer reaction in glyoxalase I (*GlxI*), in aqueous solution and in the gas phase [28]

| | KIE (H/D) | KIE (H/T) | KIE (D/T) |
|---|---|---|---|
| GlxI | 5.0 ± 1.3 | 8.4 ± 2.8 | 1.6 ± 0.2 |
| Water | 3.6 ± 0.7 | 6.4 ± 1.4 | 1.8 ± 0.2 |
| Gas-phase 6-31 + G* | 4.9 | 9.5 | 2.0 |
| Gas-phase AM1 | 5.5 | 11.6 | 2.1 |

### *3.3 Triosephosphate isomerase*

TIM reversibly catalyzes the interconversion between dihydroacetone phosphate (DHAP) and glyceraldehyde 3-phosphate (Fig. 7) [1]. The catalytic base used for proton transfer from and to the substrate C1 and C2 carbon atoms is Glu165. In the most commonly accepted mechanism for TIM the residue His95, in its neutral form, acts as a general acid/base [6]. It first protonates the C2 enolate oxygen to generate an enediol and then abstracts the proton from the C1 hydroxyl group to regenerate an enolate protonated at the other oxygen, compared to the substrate. This mechanism is supported by a considerable amount of experimental data [1] and the entire free-energy profile was calculated by MD/FEP/EVB simulations and was found to reproduce the observed rate constants [8]. There are a few other suggestions for the reaction pathway in TIM, however. One involves an intramolecular proton-transfer step between the two substrate oxygens instead of proton shuttling via His95 [7]. It was pointed out in Ref. [8] that such a mechanism would inevitably seem to have a transition state for proton transfer that is destabilized by the NH dipole of His95, in apparent disagreement with experimental studies on mutants of this residue [1]. Recent QM/MM calculations at a rather high level of theory now seem to rule out the intramolecular proton-transfer mechanism and indeed show a signifi-

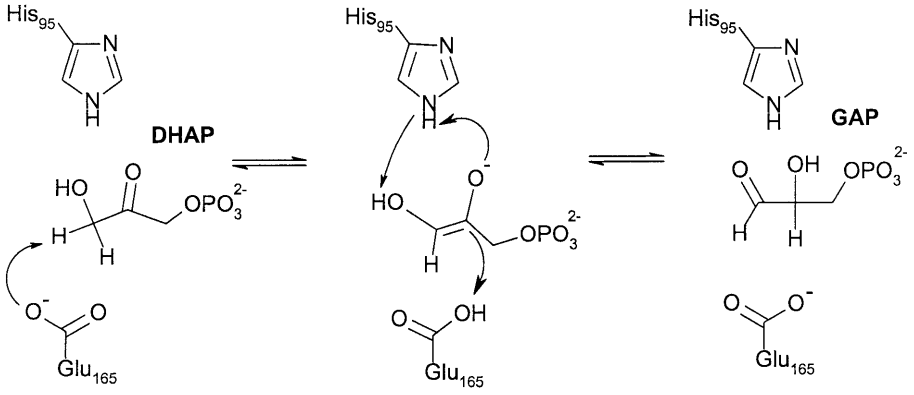


**Fig. 7.** The "imidazolate" reaction mechanism catalyzed by triosephosphate isomerase (*TIM*). The initial step involves abstraction of the C1 *pro-R* proton by Glu165. Dihydroacetone phosphate (*DHAP*) and glyceraldehyde 3-phosphate (*GAP*)

cant destabilizing effect of His95 [39]. The only remaining alternative to the classical "imidazolate" mechanism is the so-called crisscross mechanism in which Glu165 effects all the proton transfers. Such a mechanism was shown to result from mutation of His95, albeit with a much reduced rate [1]. Recent experimental studies by Harris et al. [40] gave no direct support for the crisscross mechanism but could not rule it out completely. On the other hand, it was shown that the imidazolate mechanism must be operative, at least to some extent, owing to the intramolecular transfer (via Glu165) of a tritium label from C1 to C2 [40, 41]. The calculations of Cui and Karplus [39] also essentially agree with this picture.

The rate-limiting chemical step in TIM is the initial proton abstraction from the substrate [1], which is analogous to the proton-transfer step in GlxI discussed earlier. While simulations of the entire reaction profile in TIM were reported in Ref. [8] we will limit our discussion here to the initial step which reflects the general problem in enzyme-catalyzed keto-enol isomerizations. The calculated free-energy profiles for the proton abstraction from DHAP by a glutamate in aqueous solution and in the active site of TIM are shown in Fig. 8 (details of the calculations are given in Ref. [8]). These simulations were redone here using the MD program Q [29] with a larger simulation sphere (19 Å) and longer trajectories to confirm the stability of the results and no significant differences were found. It can be seen from Fig. 8 that the free energy of the enolate form is lowered by about 15 kcal mol$^{-1}$ in the enzyme and that the transition state is stabilized by around 13 kcal mol$^{-1}$. The calculated activation free energy for proton abstraction is approximately 12 kcal mol$^{-1}$, in good agreement with experimental kinetic studies [1]. The QM/MM minimization results of Bash et al. [6] using semiempirical and Cui and Karplus [39] using density functional theory approaches are also similar to those of Fig. 8. The main difference regarding the initial proton-transfer step is that the enolate is predicted to about 5 kcal mol$^{-1}$ less stable in the QM/MM calculations of Ref. [39].

The EVB parameters used in the simulations of the TIM reaction are given in Table 2. We note that our calibrated value of the gas-phase free-energy shift, $\Delta\alpha = 34.5$ kcal mol$^{-1}$, is very similar to the gas-phase energy difference between the isolated groups in the enolate and reactant states reported in Ref. [39] with a

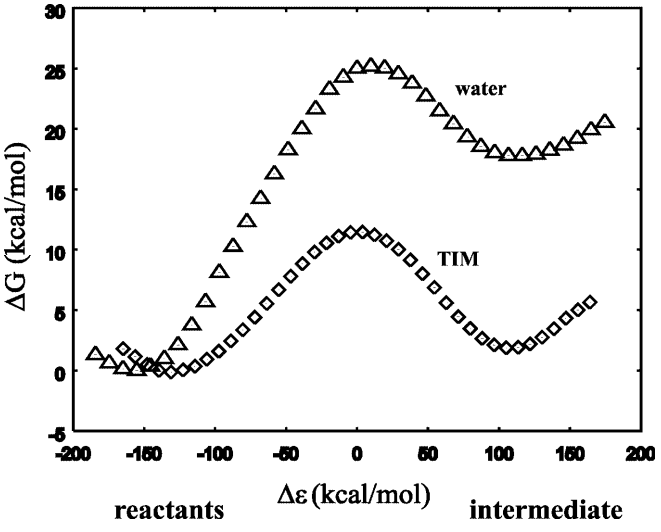


**Fig. 8.** Calculated free-energy profiles for the initial proton transfer step in TIM (*diamonds*) and for the corresponding uncatalyzed reaction in water (*triangles*)

**Table 2** Parameters used in empirical valence bond (*EVB*) simulations of the triosephosphate isomerase (*TIM*) reaction. The bond dissociation energies are taken from Ref. [43]

Morse potential: $U_{\mathrm{Morse}} = D_e\left\{1 - \exp\left[-a(b - b_0)^2\right]\right\}$

| Bond | $D_e$(kcal mol$^{-1}$) | $a$ (Å$^{-2}$) | $b_0$ (Å) |
|---|---|---|---|
| C–H | 98.8 | 1.88 | 1.09 |
| C–C | 83.1 | 2.19 | 1.53 |
| C=C | 146.9 | 1.85 | 1.39 |
| C–O$^-$ | 129.1 | 1.97 | 1.25 |
| C(O)–OH | 84.0 | 2.31 | 1.36 |
| C–OH | 84.0 | 2.18 | 1.43 |
| C=O | 174.1 | 1.86 | 1.23 |
| O–H | 110.8 | 1.84 | 1.00 |
| EVB parameters | | | |
| $\Delta\alpha$(kcal mol$^{-1}$)[a] | $H_{12}$(kcal mol$^{-1}$)[b] | | |
| 34.5 | 50.3 | | |

[a] The gas-phase energy shift was corrected by the (average) intramolecular nonbonded energies of the isolated reacting fragments, since the force field contains constant energy contributions that are not related to the actual gas-phase energy difference between the VB structures

[b] A constant off-diagonal element is used in here, while an exponential function was employed in Ref. [8]

basic model excluding the phosphate group. There a value of 32.9 kcal mol$^{-1}$ was calculated at the B3LYP/6-31+G(d,p) level, excluding thermal corrections (the values are, in principle, comparable since the phosphate group in our case is treated as part of the surrounding and is not included in the gas-phase potential). Furthermore, a calculation of the reaction free-energy profile in the gas phase (not shown), using the EVB potential calibrated in solution, yields a free-energy barrier of 23.4 kcal mol$^{-1}$ relative to the complex between the reacting groups with the resulting enolate lying about 1 kcal mol$^{-1}$ lower than the highest point on the profile (the phosphate group is again excluded from the calculation). This result is also in reasonable agreement with the corresponding potential energy difference relative to the reactant complex (excluding thermal corrections) of about 24 kcal mol$^{-1}$ reported by Cui and Karplus [39] for their basic model. The EVB model for this reaction, although parameterized against solution data, thus yields very similar gas-phase energetics for the first reaction step compared to Ref. [39]. It thus seems that the 5 kcal mol$^{-1}$ difference in stability of the enolate in the enzyme is rather related to differences in interactions with the protein and solvent. In this context, it may be worth noting that our nonbonded parameters for charged groups were calibrated by FEP simulations (including long-range electrostatics) against hydration free energies [8, 24]. Regarding the calculations reported in Ref. [39] it is also of interest that the predicted endothermicity of the reaction step in a continuum solvent was reported as 23.4 kcal mol$^{-1}$, again excluding the phosphate group. This value would imply a p$K_a$ of about 21.3 (using a p$K_a$ of 4.1 for the glutamic acid side chain). This is two units higher than that observed for acetone [13] in spite of the presence of the substrate hydroxyl group, which is expected to yield a lower p$K_a$ than acetone. Since the effect of the phosphate group is known experimentally to cause an upwards p$K_a$ shift of 1 unit [42], the p$K_a$ value for DHAP implied by the results in Ref. [39] is significantly larger than the experimental estimate of Richards [42] as well as our earlier theoretical estimate [8] for DHAP.

The first question of interest regarding the enzyme-catalyzed reaction is again how much of the activation barrier reduction in the first step of TIM can be explained simply by stabilization of the (transient) intermediate enolate anion. By the same procedure as in GlxI we hypothetically shift the gas-phase free-energy difference between reactants and products of this step so that the reaction free energy in solution coincides with that calculated for the enzyme reaction. The result is shown in Fig. 9, where it can be seen that this (hypothetical) reaction profile in solution still has an excess barrier of about 5 kcal mol$^{-1}$ compared to the enzyme reaction. Thus, out of the 14 kcal mol$^{-1}$ transition-state stabilization in the enzyme reaction, approximately 9 kcal mol$^{-1}$ can be explained by enolate stabilization, while the remaining 5 kcal mol$^{-1}$, actually 34%, is again derived from the reduction of reorganization free energy. The reorganization energies can be calculated from the diabatic free-energy surfaces as described elsewhere [8, 21] (see also later). The reduction in the reorganization energy that we obtain for the first step in TIM is about 20 kcal mol$^{-1}$, which, by the Marcus type of formula [34], predicts a barrier reduction of $\Delta\Delta G^{\ddagger} \approx \Delta\lambda/4 = 5$ kcal mol$^{-1}$, in agreement with Fig. 9.

The second question of interest is how the main part of the barrier reduction, i.e., that corresponding to stabilization of the enolate, is achieved in TIM. Here, both the QM/MM results of Bash et al. [6] and Cui and Karplus [39] and the EVB simulations show that the electrostatic interaction between Lys12 and the negative enolate oxygen dominates the catalytic effect (Fig. 10). Using the linear response approximation as for GlxI (see also Ref. [44]), it is found that Lys12 stabilizes the enolate species compared to the reactant by over 15 kcal mol$^{-1}$. Both His95 and Asn10 also contribute to the stabilization but to a much lesser extent than the lysine. These results are in accord with experimental measurements for mutants [41, 45]. It was also pointed out in Ref, [8] that the crystallographically observed

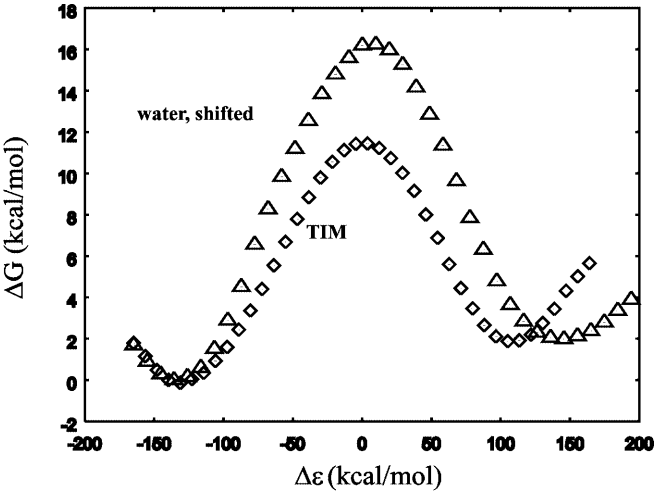


**Fig. 9.** Evaluation of the contribution of enolate stabilization to the catalytic effect in TIM. The procedure of shifting $\Delta G^0_{PT}$ for the uncatalyzed reaction is the same as in Fig. 4

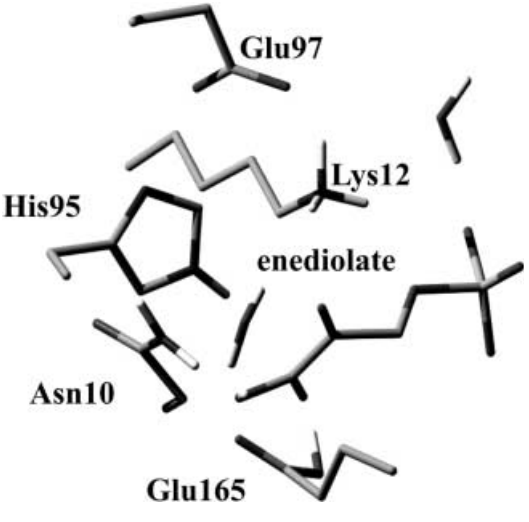


**Fig. 10.** MD snapshot of the active site of TIM after proton transfer from the substrate to Glu165

water molecule that forms a hydrogen bond to the carboxylate group of Glu165 plays a role in catalysis. Åqvist and Fothergill further predicted that the reason for the reduced activity of the S96P mutant would be related to the displacement of that water molecule, which was later indeed confirmed to be absent in the crystal structure of the mutant [46]. This active-site water can apparently interact with the "moving" negative charge during the reaction [8]. Its effect on the initial proton-abstraction step actually favors the reactant state over the enolate by about 5 kcal $mol^{-1}$ (estimated from the linear response approximation) and a similar result was reported in Ref. [39]. This might at first seem to be an "anticatalytic" phenomenon; however, it should be kept in mind that the TIM mechanism requires Glu165 to be unprotonated in the Michaelis complex, so just raising the p$K_a$ of Glu165 by desolvation (e.g., removing the water molecule) may not be a viable catalytic strategy [46].

It has often been proposed that ground-state destabilization by steric strain or desolvation may provide a major contribution to the catalytic effect. In the case of TIM, this type of proposal has been put forward by Menger [47], who suggested that the binding energy of the phosphate group could be used to destabilize the ground state by forcing the substrate into a conformation characterized by unfavorable compressive and desolvation forces. The effect of the active-site water molecule discussed previously clearly contradicts the desolvation hypothesis, which is always associated with the problem that ionized groups tend to become neutral upon desolvation [48]. In order to quantitatively examine the magnitude of strain effects on the first step in TIM, we evaluated the average intramolecular substrate energies in the enzyme and solution reactions. These results are shown in Table 3, where it can be seen that the calculated strain contribution to the transition-state stabilization in the enzyme is only $\Delta\Delta E^{\ddagger}_{strain} = -0.3$ kcal $mol^{-1}$. This value is evidently very small compared to the overall catalytic effect and we therefore conclude that the strain hypothesis in this case is not valid.

**Table 3** Calculated contribution (kcal $mol^{-1}$) from intramolecular substrate strain to the catalytic effect on the first reaction step in TIM

| | $E^0_{strain}$ | $E^{\ddagger}_{strain}$ | $\Delta E^{\ddagger}_{strain}$ |
|---|---|---|---|
| TIM | −985.9 | −957.4 | 28.5 |
| Water | −987.1 | −958.3 | 28.8 |

### *3.4 Ketosteroid isomerase*

As our final example of enzyme-catalyzed proton abstraction of the keto-enol isomerization type we consider recent calculations on KSI (3-oxo–$\Delta^5$-steroid isomerase), which is of particular interest since this enzyme has no positively charged groups in its active site. This enzyme is involved in microbial steroid metabolism and catalyzes the isomerization of $\beta$, $\gamma$-unsaturated 3-oxosteroids to their conjugated isomers via a dienolate intermediate at an almost diffusion-controlled rate [49]. The reaction is a one-base two-step proton transfer (Fig. 11), where the C4 proton is abstracted from the $\Delta^5$-3-ketosteroid by Asp40 (*Pseudomonas putida* sequence numbering). The dienolate intermediate is then reprotonated at C6 by the same residue to form the $\Delta^4$-3-ketosteroid product. Besides the general acid/base, two other polar groups, namely Asp103 (p$K_a$ > 9 [49]) and Tyr16, are found in the mostly hydrophobic active site and these two residues are within hydrogen-bonding distance to the O3 oxygen of the substrate [49, 50]. All three residues, Asp40, Asp103 and Tyr16, have also been shown to be essential for the catalytic activity [51, 52], where the latter two are believed to be involved in stabilization of the developing negative charge on O3 by hydrogen bonds [49]. The existence of LBHBs, either between Tyr16 and O3 [53] or between Asp103 and Tyr16 [54], has also been proposed as an explanation for the high catalytic efficiency of KSI.

The KSI reaction was modeled as a two-step proton transfer using MD/FEP/EVB simulations as described earlier. In this case, direct experimental information on the kinetics of the acetate-catalyzed isomerization in solution of 5-androstene-3,17-dione to the conjugate isomer protonated at C4 [55] could be used for calibration of the EVB Hamiltonian. The corresponding barriers to dienolate formation from substrate and product are 19.6 and 26.0 kcal $mol^{-1}$, respectively, after the 1M→55 M correction for bringing the donor and acceptor into contact distance in water. The free energy of the intermediate dienolate state lies 10.7 kcal $mol^{-1}$ above the reactants.

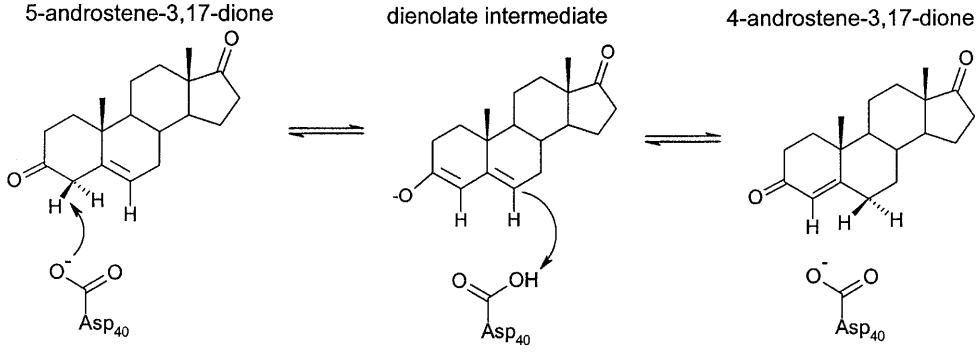


**Fig. 11.** Reaction mechanism of 3-oxo–$\Delta^5$-steroid isomerase

In order to be catalytically active Asp40 must be ionized in the Michaelis complex of the reaction. The available crystal structures of KSI in complex with relevant inhibitors [50, 56] do not, however, show any water molecules near Asp40, which raises the question of how the p$K_a$ value of the catalytic base can be kept low enough for it to be negatively charged. However, in these structures Asp40 is, in fact, mutated to Asn, whereby the negative charge is removed. Interestingly, inspection of the crystal structures reveals that there is an empty cavity adjacent to Asp40 which is of about the right size for accommodating a water molecule (Fig. 12). Such a water molecule would stabilize the negative charge of Asp40 and can also engage in hydrogen bonding with Tyr57. It turns out that MD simulations reproduce the KSI structure in complex with a substrate both with and without such a water molecule. On the other hand, the results from FEP calculations show that introduction of the active-site water stabilizes the negative charge of Asp40 in the enzyme-substrate complex by about 5 p$K_a$ units. While is it somewhat tricky to calculate the absolute p$K_a$ value of Asp40, owing to uncertainties in where the proton would be positioned in the neutral form, our preliminary results indicate that the p$K_a$ of Asp40 is significantly shifted upwards from its solution value when no water molecule is present in the active site. Note that the experimental p$K_a$ of this residue is 4.6 in the free enzyme and 4.7 in the Michaelis complex [57], i.e., in both cases close to its unperturbed value. In view of these considerations we decided to carry out the EVB simulations of KSI both with and without the putative water molecule present.

The results of these calculations are shown in Fig. 13 together with the experimental free-energy profile for the *Pseudomonas testosteronii* enzyme [58] and that of the calibrated solution reaction. It appears that the thermodynamics of the entire reaction is best reproduced with the water molecule occupying the active-site cavity. In fact, these calculations are in almost perfect agreement with the experimental data, the only difference being that the reprotonation step has a barrier that is too high by about 3 kcal mol$^{-1}$. The EVB simulations without any water molecule in the internal cavity yield a free-energy profile that is also in reasonable agreement with the experiments. The profile in this case is mainly characterized by an overstabilization of the dienolate intermediate by about 3 kcal mol$^{-1}$ compared to the experimental value and the flanking activation barriers are accordingly also somewhat underestimated. This result is basically in agreement with our predictions regarding the effect of the active-site water on the p$K_a$ of Asp40. Note, however, that the water molecule also has a stabilizing effect on the negative charge on the dienolate, so it is the relative p$K_a$ difference between Asp40 and the substrate which is shifted by 2 units in favor of the protonated aspartic acid when the molecule is not present. This is thus best characterized as a ground-state desolvation effect and it seems questionable whether Asp40 really would be ionized in the Michaelis complex in this case. Furthermore, the good agreement between the calculated and the observed equilibrium constants for the case with the active-site water molecule present speaks in its favor together with fact that empty cavities adjacent to carboxylate groups in proteins are most unusual.

In any case, it is clear that the enzyme lowers the free-energy barrier of the initial proton abstraction by around 10 kcal mol$^{-1}$ and also stabilizes the dienolate by a similar amount. By performing the same analysis as described earlier for GlxI and TIM we find that the reduction of the activation barrier in KSI has a contribution of about 60% from stabilization of the dienolate intermediate and the remaining 40% is from the reduction of the reorganization energy (these relative

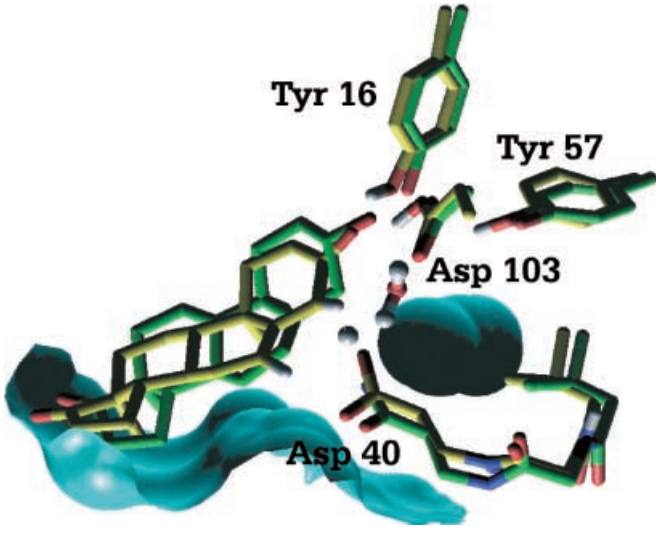


**Fig. 12.** Snapshot from MD simulations of the ketosteroid isomerase (*KSI*) reaction in the intermediate enolate state after proton transfer to Asp40. Superimposed on the MD structure (*yellow*) is the crystallographic complex [56] of the Asp40Asn mutant of the *Pseudomonas putida* enzyme with substrate (*green*). Part of the outer molecular surface together with the internal cavity for the experimental structure is also shown

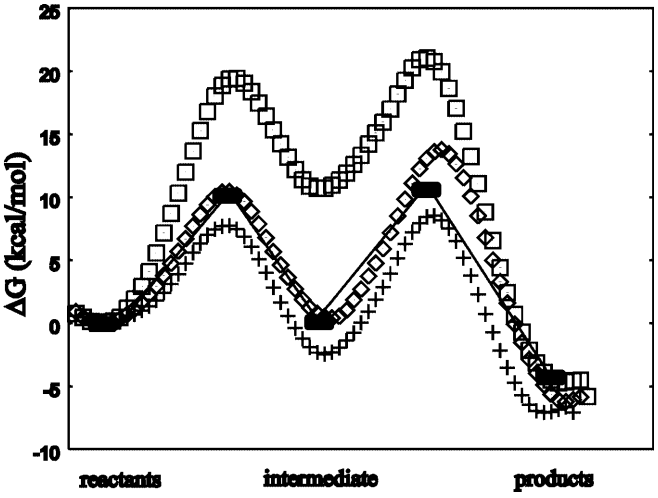


**Fig. 13.** Calculated free-energy profiles for the catalytic reaction in KSI, both with (*diamonds*) and without (*crosses*) the internal water molecule present, and for the uncatalyzed reaction in water (*squares*). Experimental results for the *Pseudomonas testosteronii* enzyme are shown as *solid lines* [58]

contributions are interestingly the same with and without the active-site water). The calculated diabatic (diagonal) free-energy curves for the proton abstraction step in enzyme and in solution are shown in Fig. 14, which directly demonstrates the reorganization energy reduction effect, $\Delta\lambda \approx 20$ kcal mol$^{-1}$. With the calculated reorganization energies from Fig. 14 one can also examine the validity of the Marcus type of formula modified for abdiabatic reactions [34]:

$$\Delta G^{\ddagger} \approx \left(\Delta G^0 + \lambda\right)^2/4\lambda - \bar{H}_{12}\left(X^{\ddagger}\right) + \bar{H}_{12}^2(X_0)/\left(\Delta G^0 + \lambda\right) \quad . \tag{8}$$

Insertion of the relevant quantities ($\Delta G^0$, $\lambda$ and the $H_{12}$s) into this equation, in fact, predicts the activation free energies of Fig. 13 quite accurately. For another recent discussion of such free-energy relations see Ref. [59]. The calculation of diabatic free-energy surfaces in the context of QM/MM simulations has also recently been addressed by Mo and Gao [60], who present an interesting method for combining molecular orbital calculations with a VB framework by using a block-localized wave function approach.

The simulations of the KSI reaction confirm the hypothesis that the major catalytic factor is hydrogen bonding to the negative dienolate oxygen by Asp103 and Tyr16. Furthermore, the results support the hydrogen-bonding pattern favored by Pollack et al. [49] where these two residues simultaneously donate hydrogen bonds to the substrate, in both transition states as well as in the dienolate intermediate (Fig. 12). Analysis of the energetics using the linear-response approximation yields an overall contribution of about 9 kcal mol$^{-1}$ to the stabilization of the dienolate from Tyr16 and Asp103, which are the most important residues in this respect. These results are in accord with experimental studies of Tyr16 and Asp103 mutants [61].

Since LBHBs have been proposed as a possible catalytic factor in KSI we also addressed the energetics associated with hydrogen bonding between Tyr16 and the substrate using EVB simulations. Both tyrosine and the enol form of the substrate have p$K_a$ values of 10.0 in solution [55], which might suggest that the two groups could form an LBHB in the intermediate state or at the flanking transition states, since p$K_a$-matching of the proton donor and acceptor groups is considered a prerequisite for such interactions [4, 5]. The results of MD/FEP/EVB calculations of the proton-transfer profile between the tyrosine and the dienolate form of the substrate in water, in KSI and in the gas-phase are shown in Fig. 15. The solution reaction was calibrated as usual against experimental data, where the effective barrier (including tunnellng and ZPE effects) is predicted to be about 4.5 kcal mol$^{-1}$ from accurate free-energy relationships [62]. The gas-phase proton-transfer profile resulting from this model shows, as expected, a reduced barrier that is now about 2.5 kcal mol$^{-1}$ and a slight endothermicity of about 1.3 kcal mol$^{-1}$ for transfer of the proton to the dienolate acceptor. The strength of the hydrogen bond in a vacuum is about −18 kcal mol$^{-1}$ with a donor–acceptor (O–O) distance of 2.49 Å and a mixing coefficient corresponding to approximately 16% covalent bonding to the acceptor (i.e., the second resonance form of Eq. 1). In water the hydrogen bond has a donor–acceptor distance of 2.8 Å and only 6% mixing of the second resonance form. Thus, even without any specific parameterization of this model against gas-phase data the EVB Hamiltonian reproduces the main characteristics of a strong gas-phase hydrogen bond, or LBHB, through calibration against solution experiments. Of course, it would be possible to fit an EVB surface directly to experimental gas-phase data or ab initio calculations on a relevant hydrogen-bonded complex in a vacuum, but for our present purposes this is not necessary.

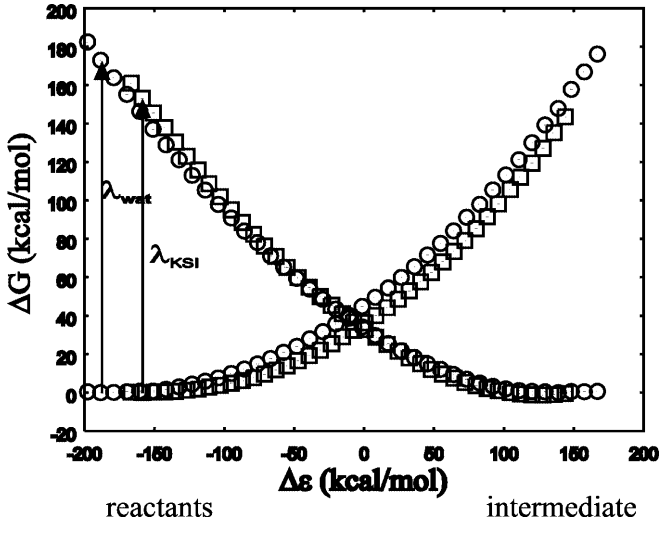


**Fig. 14.** Calculated diabatic (diagonal) free-energy functions for the initial proton-transfer step in KSI (*squares*) and for the uncatalyzed reaction in water (*circles*). The product curves have been shifted so that the reorganization energies are directly given by the energy gaps at the reactant minima

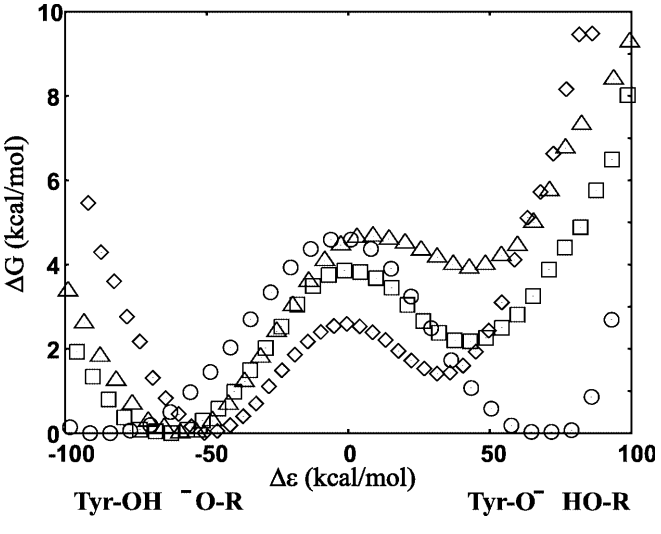


**Fig. 15.** Calculated free-energy profiles for proton transfer between tyrosine (Tyr16 in KSI) and the substrate dienolate in aqueous solution (*circles*), in the gas-phase (*diamonds*) and in the active site of KSI with (*squares*) and without (*triangles*) the internal water molecule present

Having verified that the tyrosine–dienolate hydrogen bond has the required properties both in solution and in a vacuum the effect of the enzyme environment on this interaction can be examined. The calculated proton-transfer free-energy profiles between Tyr16 and the enolate oxygen both with and without the extra water molecule in the active site of KSI are shown in Fig. 15. It can be seen that localization of the proton on Tyr16 is clearly favored in the enzyme and that the barriers to proton transfer are predicted to be higher than in the gas phase. For the enzyme profile that includes the active-site water molecule, we observe an endothermicity that is in excellent agreement with the reported p$K_a$ shift of 1.6 p$K_a$ units = 2.2 kcal mol$^{-1}$ for Tyr16 in KSI (this p$K_a$ has been reported as 11.6 [53]). The anionic hydrogen bond is, however, strengthened in the enzyme compared to aqueous solution, with the donor–acceptor distance being 2.6 Å and 12% mixing with the covalent donor–hydrogen resonance form. Experimentally, this hydrogen bond appears to be worth approximately 5 kcal mol$^{-1}$ for catalysis [61]. While this is clearly both a short and a strong ionic hydrogen bond there seems to be nothing particularly "magic" about it. Like all strong hydrogen bonds, it has a significant degree of covalent character [16, 63, 64] but its strength derives mainly from electrostatic attraction [65]. Furthermore, we note that the p$K_a$s in the enzyme are not perfectly matched, that the preferred location of the proton is on Tyr16 and not on the dienol(-ate) and that the catalytic contribution from the hydrogen bond is far from the 20 kcal mol$^{-1}$ hypothesized for LBHBs. Thus, by these standards it cannot be considered to be an LBHB, according to the original definition of the concept [4].

A few ab initio studies of model systems related to the KSI reaction have also been reported recently [66, 67]. The strategy followed in these works is to carry out fairly high level calculations on simplified systems typically encompassing a model of the substrate and 2–4 of the catalytic groups in the enzyme. Although polarization effects of a surrounding dielectric medium were treated in Refs. [66, 67] this was in both cases done only through single-point calculations on geometries optimized in a vacuum, which necessarily renders more gas-phase-like structures. The work of Kim et al. [66], which addressed the reaction path of KSI, neither yielded the same rate-limiting step as observed experimentally nor did it reproduce the activation barriers. The results reported in Refs. [66, 67] were considered to support the LBHB mechanism in KSI, apparently mainly because short hydrogen bonds (2.5–2.6 Å donor–acceptor distance) were obtained. However, in both of the studies the proton was clearly localized on one of the heavy atoms. The study by Pan and McAllister [67] did not address the reaction profile but only the relative stabilities of different hydrogen-bonded complexes. In that case, the most stable structure underwent essentially complete proton transfer from phenol (Tyr16) to butadienolate (substrate) and from formic acid (Asp103) to phenol. This type of situation with three concerted proton transfers involved in reaching the reaction intermediate seems highly unlikely and disagrees both with the crystallographic structures [50] and those from the present simulations, where double hydrogen bonding (from Asp103 and Tyr16) to the dienolate is observed. As noted earlier, the p$K_a$ of Tyr16 is also shifted upwards to 11.6 [53], which indeed suggests that it will remain protonated.

## 4 Discussion

The high turnover rates of enzymes that catalyze proton abstraction from carbon atoms adjacent to a carbonyl/carboxylate group have been considered as a fundamental problem in enzymology, since these reactions are usually very slow in solution. As briefly discussed in the Introduction, a number of possible origins for the efficient catalysis of such proton-transfer steps have been proposed on the basis of interpretations of experimental data [2, 3, 4, 5]. On the other hand, there have been relatively few, if any, attempts to explain the general principles of these reactions by comparative theoretical calculations. This may seem somewhat surprising in view of the recent advances in modeling enzyme reactions with EVB and QM/MM methods that take into account the reaction environment in a realistic manner. A number of case studies of specific enzyme reactions of the keto-enol isomerzation type have, however, been reported that demonstrate the power of these techniques for elucidating the details of catalysis [6, 7, 8, 9, 10, 11, 12, 28, 39]. In our opinion, to settle the issue of the origin of catalysis in these enzymes it is not only useful but also necessary to employ properly validated theoretical approaches, since the detailed energetics can hardly be dissected by experimental means.

Here we have discussed MD/FEP/EVB simulations of three different enzymes catalyzing keto-enol like isomerization steps. We find it very convincing that the simulations essentially reproduce the available experimental energetics for these enzymes, which clearly demonstrates the power of the simulation approach. The general principles that emerge from the calculations are that two main factors are responsible for the catalytic rate enhancement of these reactions: stabilization of the negatively charged enolate species by electrostatic interactions, including strong ionic hydrogen bonding; and reduction of the reorganization energies associated with the proton transfer by preoriented dipolar groups of the active site (these two effects were also discussed and demonstrated in Ref. [8]).

The electrostatic stabilization of the enolate form can apparently be achieved in different ways. In GlxI the divalent cation plays the main role, while in TIM it is a positively charged lysine residue, but in both cases the overall stabilization of the enolate is the same, about 15 kcal mol$^{-1}$. On the other hand, in KSI the stabilization is effected mainly by two strong hydrogen bonds, those from Tyr16 and Asp103. The calculated (and observed) lowering of the free energy of the intermediate state is, however, somewhat smaller (10 kcal mol$^{-1}$) in KSI compared to the other two enzymes. While this may possibly reflect a limit for what can be done by just two hydrogen bonds, it is of course the activation barrier that matters and the three enzymes end up with

approximately the same rate constants. It may also be of significance that in all three cases the free energy of the enolate form is brought to just about the same level as that of the reactant, i.e., with a $\Delta G^0_{PT}$ close to zero. For reactions with overall equilibrium constants close to unity this makes sense from the viewpoint of evolutionary optimization as was discussed early on by Albery and Knowles [68].

The second important part of the catalytic effect is the reduction of the reorganization energy accompanying proton abstraction from the keto form of the substrate. While this type of phenomenon had been hypothesized by several authors [4, 65, 69], it is only through recent EVB simulations that the existence of the effect has been proven [8, 34, 70]. It may be noted that the reorganization energy is less straightforward to quantify in molecular orbital QM/MM models since free-energy surfaces that do not correspond to the ground state are much more difficult to evaluate by such methods (see, however, the recent study by Mo and Gao [60]). This may be a reason for why the effect never seems to have been uncovered in such QM/MM studies. The magnitude of the influence of the reduction of the reorganization energy on the activation barrier can be assessed by calculating the diabatic free-energy surfaces and inserting the resulting reorganization-energy shift into the Marcus equation. However, we find that the idea to artifically shift the gas-phase free energy of the uncatalyzed solution reaction, so that $\Delta G^0_{PT}$ becomes identical in the hypothetical solution reaction and in the enzyme, is a more accurate approach [8].

It is interesting and maybe of significance that the portion of the overall transition-state stabilization due to the reduction of the reorganization energy is 30%, 34% and 40% in GlxI, TIM and KSI, respectively. That is, it seems possible, judging from these admittedly few data points, that there is a correlation between the magnitude of the reduction of the reorganization free energy and the specific nature of electrostatic interactions (including hydrogen bonds) between the substrate and the active site.

Several other hypotheses invoked as explanations for the high catalytic turnover rates of enzymes catalyzing keto-enol isomerizations were also examined here. In the case of GlxI, the influence of quantum mechanical tunneling and zero-point motion was examined using the path integral technique. While such effects are found to make a substantial contribution to the absolute reaction rates, corresponding to a lowering of the apparent free-energy barrier of about 2.5 kcal $mol^{-1}$ compared to the classical case, they are virtually identical in the enzyme and in solution. At least in GlxI, quantum effects are thus not of importance for the catalytic power of the enzyme. In the case of TIM, we evaluated the magnitude of the substrate strain contribution to the activation energy and found this to be very small. Such strain effects have been proposed to be important in this enzyme [47], but the present results provide evidence to the contrary. It is also sometimes argued that ground-state destabilization by desolvation of the catalytic carboxylate base in enzymes such as TIM and KSI would provide a catalytic advantage, since the p$K_a$s of the base and substrate would become more closely matched. There is, however, a trivial limitation to such a catalytic strategy since the general base actually needs to be deprotonated for catalysis.

The existence of LBHBs has also been suggested to be of major importance for the class of enzymes that we are dealing with [4, 5, 53, 54]. The experimental results invoked as evidence for this hypothesis are typically highly deshielded proton NMR signals and short donor–acceptor distances observed in crystal structures. While the interpretation of NMR spectra is a matter of some debate, convincing evidence for the relevant protons being delocalized between the donor and acceptor atoms seems to be lacking [16]. Moreover, the predicted stabilization of more than 20 kcal $mol^{-1}$ allegedly provided by LBHBs [4, 5] has never been observed experimentally in enzymes. The present calculations show that in KSI the preferred proton location in the hydrogen bond between Tyr16 and the dienolate is on the tyrosine and that $\Delta pK_a$ between these groups is actually not zero in the enzyme. QM/MM calculations on other enzymes of this category have also reached the conclusion that LBHBs are not of importance for catalysis of these reactions [9, 10]. A consistent picture thus seems to emerge from calculations that take into account more than a few groups in the gas phase or in a low-dielecric continuum.

The present MD/FEP/EVB computational model is able to correctly predict a number of relevant features of the reactions of GlxI, TIM and KSI studied: reaction rate and equilibrium constants, effects of metal ion substitutions and of amino acid mutations, KIEs, p$K_a$ shifts of catalytic groups, etc. It is thus clear that computational methods of this type (EVB or QM/MM), where the entire system involved in catalysis is treated in a realistic microscopic way, can provide invaluable information about specific reaction mechanisms as well as general principles of enzyme catalysis.

*Acknowledgements*. Support from the Swedish Research Council and the National Graduate School of Scientific Computing is gratefully acknowledged.

## References

1. Knowles JR (1991) Nature 350: 121
2. Gerlt JA, Gassman PG (1992) J Am Chem Soc 114: 5928
3. Guthrie JP, Kluger R (1993) J Am Chem Soc 115: 11569
4. Gerlt JA, Gassman PG (1993) J Am Chem Soc 115: 11552
5. Cleland WW, Kreevoy MM (1994) Science 269: 102
6. Bash PA, Field MJ, Davenport RC, Petsko GA, Ringe D, Karplus M (1991) Biochemistry 30: 5826
7. Alagona G, Ghio C, Kollman PA (1995) J Am Chem Soc 117: 9855
8. Åqvist J, Fothergill M (1996) J Biol Chem 271: 10010
9. Mulholland AJ, Lyne PD, Karplus M (2000) J Am Chem Soc 122: 534
10. Donini O, Darden T, Kollman PA (2000) J Am Chem Soc 122: 12270
11. Feierberg I, Cameron AD, Åqvist J (1999) FEBS Lett 453: 90
12. Alhambra C, Gao J, Corchado JC, Villa J, Truhlar D (1999) J Am Chem Soc 121: 2253
13. Chiang Y, Kresge AJ, Tang YS, Wirz J (1984) J Am Chem Soc 106: 460
14. Warshel A, Papazyan A (1996) Proc Natl Acad Sci USA 93: 13665

15. Guthrie JP (1996) Chem Biol 3: 163
16. Ash EL, Sudmeier JL, De Fabo EC, Bachovchin WW (1997) Science 278: 1128
17. Shan SS, Loh S, Herschlag D (1996) Science 272: 97
18. Gerlt JA, Kreevoy MM, Cleland WW, Frey PA (1997) Chem Biol 4: 259
19. Chen JC, McAllister MA, Lee JK, Houk KN (1998) J Org Chem 63: 4611
20. Warshel A (1991) Computer modeling of chemical reactions in enzymes and solutions. Wiley, New York
21. Åqvist J, Warshel A (1993) Chem Rev 93: 2523
22. Chang Y-T, Miller WH (1990) J Phys Chem 94: 5884
23. Luzhkov V, Åqvist J (1998) J Am Chem Soc 120: 6131
24. Åqvist J, Fothergill M, Warshel A (1993) J Am Chem Soc 115: 631
25. Luzhkov V, Åqvist J (1999) Chem Phys Lett 302: 267
26. Voth GA, Chandler D, Miller WH (1989) J Chem Phys 91: 7749
27. Hwang J-K, Warshel A (1996) J Am Chem Soc 118: 11745
28. Feierberg I, Luzhkov V, Åqvist J (2000) J Biol Chem 275: 22657
29. Marelius J, Kolmodin K, Feierberg I, Åqvist J (1998) J Mol Graph Model 16: 213
30. Vander Jagt DL (1989) In: Dolphin D, Poulson R, Avramovic O (eds) Coenzymes and cofactors, vol 3A. Wiley, New York, p 597
31. Cameron AD, Ridderström M, Olin B, Kavarana MJ, Creighton DJ, Mannervik B (1999) Biochemistry 34: 2788
32. Kohen A, Klinman JP (1998) Acc Chem Res 31: 397
33. Hwang J-K, Chu ZT, Yadav A, Warshel A (1991) J Phys Chem 95: 8445
34. Warshel A, Hwang JK, Åqvist J (1992) Faraday Discuss 93: 225
35. Garcia-Viloca M, Alhambra C, Truhlar DG, Gao J (2001) J Chem Phys 114: 9953
36. Vander Jagt DL, Han L-PB (1973) Biochemistry 12: 5161
37. Schimandle CM, Vander Jagt DL (1979) Arch Biochem Biophys 195: 261
38. Swain CG, Stivers EC, Reuwer JF Jr, Schaad J (1958) J Am Chem Soc 80: 5885
39. Cui Q, Karplus M (2002) J Phys Chem B 106: 1768
40. Harris TK, Cole RN, Comer FI, Mildvan AS (1998) Biochemistry 37: 16828
41. Nickbarg EB, Davenport RC, Petsko GA, Knowles JR (1988) Biochemistry 27: 5948
42. Richard JP (1984) J Am Chem Soc 106: 4926
43. Dickerson RE, Gray HB, Haight GP Jr (1979) Chemical principles. Benjamin/Cummins, Menlo Park, Calif
44. Åqvist J, Hansson T (1996) J Phys Chem 100: 9512
45. Lodi PJ, Chang LC, Knowles JR, Komives EA (1994) Biochemistry 33: 2809
46. Zhang Z, Komives EA, Sugio S, Blacklow SC, Narayana N, Xuong NH, Stock AM, Petsko GA, Ringe D (1999) Biochemistry 38: 4389
47. Menger FM (1992) Biochemistry 31: 5368
48. Warshel A, Åqvist J, Creighton S (1989) Proc Natl Acad Sci USA 86: 5820
49. Pollack RM, Thornburg LD, Wu ZR, Summers MF (1999) Arch Biochem Biophys 370: 9
50. Kim SW, Cha S-S, Cho H-S, Kim J-S, Ha N-C, Cho M-J, Joo S, Kim KK, Choi KY, Oh B-H (1997) Biochemistry 36: 14030
51. Kuliopulos A, Mildvan AS, Shortle D, Talalay P (1989) Biochemistry 28: 149
52. Wu ZR, Ebrahimian S, Zawrotny ME, Thornburg LD, Perez-Alvarado GC, Brothers P, Pollack RM, Summers MF (1997) Science 276: 415
53. Zhao Q, Abeygunawardana C, Talalay P, Mildvan AS (1996) Proc Natl Acad Sci USA 93: 8220
54. Zhao Q, Abeygunawardana C, Gittis AG, Mildvan AS (1997) Biochemistry 36: 14616
55. Zeng B, Pollack RM (1991) J Am Chem Soc 113: 3838
56. Ha N-C, Kim M-S, Lee W, Choi KY, Oh B-H (2000) J Biol Chem 275: 41100
57. Pollack RM, Bantia S, Bounds PL, Koffman BD (1986) Biochemistry 25: 1905
58. Hawkinson DC, Eames TCM, Pollack RM (1991) Biochemistry 30: 10849
59. Kiefer PM, Hynes JT (2002) J Phys Chem A 106: 1834
60. Mo Y, Gao J (2000) J Comput Chem 21: 1458
61. Choi G, Ha N-C, Kim SW, Kim D-H, Park S, Oh B-H, Choi KY (2000) Biochemistry 39: 903
62. Eigen M (1964) Angew Chem Int Ed Engl 3: 1
63. Coulson CA, Danielsson U (1954) Ark Fys 8: 239
64. Cornilescu G, Hu J-S, Bax A (1999) J Am Chem Soc 121: 2949
65. Warshel (1978) Proc Natl Acad Sci USA 75: 5250
66. Kim KS, Oh KS, Lee JY (2000) Proc Natl Acad Sci USA 97: 6373
67. Pan Y, McAllister MA (2000) J Mol Struct (THEOCHEM) 504: 29
68. Knowles JR, Albery WJ (1977) Acc Chem Res 10: 105
69. Albery WJ (1980) Annu Rev Phys Chem 31: 227
70. Yadav A, Jackson RM, Holbrook JJ, Warshel A (1991) J Am Chem Soc 113: 4800